University of Thi-Qar Journal of Science (UTJsci)
E-ISSN: 2709-0256, P-ISSN: 1991-8690, Vol. 10, No. 2, Dec. 2023

Role of magnetic nanoparticles incorporation for the enhanced efficiency of ZnO based Dye-Sensitized Solar Cells (DSSCs)

[1st] Noor Abdulsalam
Dept. of Physics/ College of Science/ University of Basrah
Iraq/Basrah
abdallahnoor615@gmail.com

[2nd] Basil A. Abdullah
Dept. of Physics/ College of Science University of Basrah
Iraq/Basrah
basil.abdullah@uobasrah.edu.iq

[3rd] Hashim Jabbar
Dept. of Physics/ College of Science University of Basrah
Iraq/Basrah
hashim.jabbar@uobasrah.edu.iq

Received: 2023-08-17, Revised: 2023-09-07, Accepted: 2023-09-19, Published: 2023-12-25

Abstract—**In this study, we reported on the effect of the internal magnetic field arising from magnetic particles added to zinc oxide in certain proportions, which led to an improvement in the performance of the dye solar cell, We found that the magnetic effect It is the main factor that improves the ability to transfer electrons generated from the separation process between (electron-hole) pairs, And reduce the process of reunification between electrons and holes, The efficiency of the cell with a pure electrode was (1.38%), while the highest efficiency we got after doping was when doping with a ratio (97%ZnO+3%$MnCoFeO_4$) reached (1.7%), i.e. the percentage increase in efficiency (23%).**

***Keywords*— Dye sensitized solar cells, Zno nanoparticles, magnetic Field effect, $MnCoFeo_4$, Ferrimagnetism**

I. INTRODUCTION

It remains highly challenging to harness forms like electricity. The main solar energy conversion solar energy and transform it into useful technologies used to gather solar energy is photovoltaic devices. By producing and then gathering electron-hole pairs, these photovoltaic devices, more commonly referred to as solar cells; transform the incident photon energy of solar radiation into electrical energy. For the research and development of solar cell technology to be a practical response to our energy issue, a number of obstacles must be overcome such as high efficiency of power conversion, low price, stable for the long run, making use of plentiful and biocompatible basic resource. Based on their efficiency and cost, solar cells are divided into three generations. 1st is the p-n junction of a doped semiconductor, expensive but dominates the business market. The second Generation of solar cells is thin film solar cells built on CdTe or CuInGaSe. Although they are less efficient, they are far less expensive to make and require a simpler construction technique[1][2]. The limitation of both the first and second generations due to the Shockley-Queasier theoretical limit of 30% for a single p-n junction is an obstacle. Any solar cells that are not categorized into the 1st or 2nd generation categories are classified as 3rd Generation solar cells. By which they using wide range of technologies and are not constrained by the Shockley- Queasier limit [3], Dye sensitized solar cell is an organic solar cell of the 3rd generation. Despite having lower power conversion efficiency than other 1st and 2nd generation inorganic solar cells, DSC offers several advantages over them. DSC efficiency is almost temperature independent in the typical operating temperature range of 25-650 C. The efficiency of Si solar cells decreases by 20% [4] across the same range, (DSSCs) are distinguished by its ease of manufacture and production, as it is environmentally friendly, non-toxic, and has a low cost, and its materials are available[5], Fig(1) shows the parts of a cell. Compared to polycrystalline Si solar cells DSC exhibits even greater efficiency under diffuse sunlight or overcast circumstances. A solar tracking system is less necessary because performance is less dependent on the angle at which the light radiation is incident. Although DSC has no accessible and biocompatible. Without encountering difficulties with the supply of raw materials, the technology can be developed up to the terawatt scale. As a result, organic solar cells outperform the two main thin-film photovoltaic technologies that are in direct competition. Long-term stability is a crucial requirement for all types of solar cells. It has been proven via numerous comprehensive studies that DSCs may satisfy the stability standards necessary for

https://doi.org/ 10.32792/utq/utjsci/v10i2.1108

commercial solar cells to operate outside for more than 20 years[6][2],The purpose of this project is to include magnetic nanoparticles into ZnO photoanodes in order to enhance the photoanode's functionality via the influence of magnetism yet been put into large commercial production, it may be assumed that it will be more affordable than all thin film devices. Only inexpensive and widely available materials are required. DSC can bypass the expensive and energy-intensive high vacuum as well as materials purification processes, unlike amorphous silicon, CdTe, or CIGS cells.

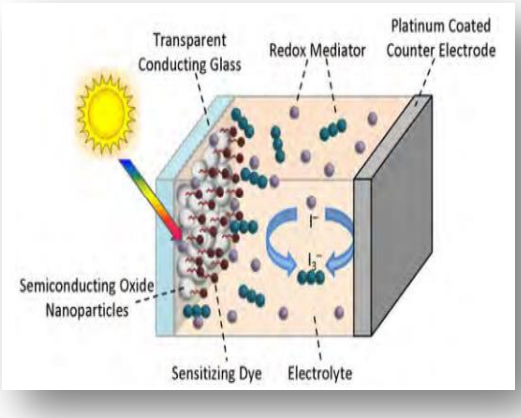

Fig.1: Schematic illustration of a typical dye-sensitized solar cell (DSSC)

II. Experimental

A. Materials

The materials used in the study are ZnO-np(*>100nm*), Ethanol (*99%*), acetylacetonate were all provided from Sigma-Aldrich. Manganese Chloride (*$MnCl_2.4H_2O$*), Cobalt Chloride(*$CoCl_2.6H_2O$*), Iron Chloride *($FeCl_3$)*,Sodium Oxidanide (*NaOH*) were all provided from (Merk) Nitric acid (*HNO_3,95%*), Isopropanol(*2P,99%*), Acetone (99%) were all abstained from scharlau. Trition X-100(98%) ,Acetylacetone (99%) and Chloroplatinic acid ($H_2ptcl_6.H_2O$) were all abstained from (*CDH*), FTO (surface resistance (11-15) Ω) and N719 (*W.M1188.55g/mole*) were all abstained from Ossila, Iodolyte Z-100 was purchased from Solar nix and deionized water.

B. Characterization devices

For image analysis, samples of nanoparticles were set up into a FE-SEM Supera Zeiss Model and scanned ata magnification of 50 k. The XRD analysis of the prepared sample of pure and doped ZnO nanoparticles, and data was collected for the 2θ range of 10° to 80° with a step of 0.1972°. Nanoparticles were done using a XRD-Rigaku diffractometer, Cu-Kα X-rays of wavelength λ=1.5406 Å. The results supported the presence of nanoscale ZnO powder. We recorded the absorption spectra of the samples with a visible-NIR spectrometer (Shimadzu UV-1800 PC). Magnetic characterizations were conducted by using Vibrated Sample Magnetometer (VSM-MDK Iran). The solar cell measurements as current-voltage characteristics of the prepared DSSC cells were conducted with a Keithley source meter 2400 (SCIENCE TECH) and solar simulator lamp AM1.5 systems with illumination of 100 "mW/cm^2".

C. Preparation of MnCoFeO4 particles

0.005 M of $MnCl_2$.4H2O was dissolved in 50 ml of deionized water, 0.005 M of $CoCl_2.6H_2O$ was dissolved in 50 ml of deionized water, and 0.01 M of $FeCl_3$ was dissolved in 250 ml of deionized water. The three solutions were mixed with continuous stirring at a temperature of 65 °C. After that, 100 ml of 0.8M NaOH solution was added dropwise to the mixed solution with continuous stirring until the pH equalized. The precipitate formed was separated and washed several times with deionized water via centrifugation. The precipitate was dried at 100 °C.

D. Preparation of ($ZnO/MnCoFeO_4$) Films

The following procedure was used to prepare the pure and doped (ZnO). A homogenous zinc oxide paste were fabricate by following procedure[7],we blend 0.1 g of (np-ZnO) with 0.02 ml of (acetyl acetone), 20 µl of (*Triton X-100*), two drops of were mixed with Nitric acid ethanol (*PH=3*), and finally, the combination were mixed thoroughly for 10 minutes. The same procedure was used to fabricate doped zinc oxide films with different ratios (*1,2,3,4,5*) % from (*$MnCoFeO_4$*), the previous pasts were coated on pre-cleaned *(FTO*) by doctor blade technique using Scotch tape (*thickness about 1 µm*). the films were air dried and then sintered at 450 °C for 30 minutes, after removing the films from the oven, its immersed in a (*N719*) dye solution of concentration 0.5 "mM" for 24 hours, after that it is carefully washed with ethanol until the inhomogeneous dye with the paste is removed and dried in air.

E. Preparation of counter electrode

$H_2PtCl_6 \cdot 6H_2O$ was dissolve Dina 1:1 mixture of isopropanol and n-butanol at concentrations of 0.25 wt%[8]The appropriate $H_2PtCl_6 \cdot 6H_2O$ solution was stirred for 6 h at room temperature and then sprayed onto the FTO substrate to give an electrode with an active area of 1 "cm^2". After blow-drying at room temperature, the substrates were heated at 200 C for 10 minutes.

III. Results and Discussion

A. SEM analysis

The sample surfaces were analyzed using SEM images of both bulk and ground ZnO nanoparticle powder following deposition on glass slides and thermal treatment at a temperature of 450 °C to determine the shape, estimate the size, and provide an overview the surface. The SEM images taken both before and after doping process are shown in Fig (2), together with histograms demonstrating the particle size distribution of ZnO nanoparticles for each image. We observed that, even after heat treatment, the morphology of the particles remains unaltered. A decrease in particle size was observed after doping with magnetic materials, which may have been caused by the manual grinding of ZnO and (*MnCoFeO4*), which shows good contact between ZnO and the impurity despite only being prepared by using a simple physical mixing method. For the platinum film, the heating process on chloroplatinic acid dissolved in isopropyl alcohol was sufficient to breakdown chlorine and transform (Pt) ions into (Pt) NPS, as a result, particles increased and agglomerated. Using the image analysis tool Image-J, we were able to estimate a large number of particle sizes from the exhibited micrographs and collect the size distribution histograms that accompany into each image in order to achieve an appropriate statistical interpretation of the data. A Log-Normal function was used to fit the histograms (continuous red line) for each size distribution.

B. XRD analysis

The pure zinc oxide sample's hexagonal structure and great crystallinity are seen in the (*XRD*) graphs, which are denoted by the presence of large and distinct peak, We notice the appearance of peaks at angles (*31.7, 34.4, 36.2, 47.5, 56.6*) degrees, and the preferred growth direction is at (101) (*2ϑ = 36.2 "degrees"*). as shown Fig:3a patterns [9]However, when the peaks are doped with *(MnCoFeO4*), the height of the peaks falls, indicating low crystallization in the compound as a result of the dopingas the highest height in the case of pure ZnO reached (31316.6)a.u, and in the case of doping with MCF, the highest height of reached (19615.4) a.u, In addition, no distinguishable peaks were seen for the doping materials, indicating the high purity of zinc oxide[10] ,Additionally, doping only has the impact of weakening the crystal development of (*ZnO*) as shown Fig:3b, powder (*MnCoFeO4*) platinum film deposited on glass were also measured as shown" Fig(3)" c,d.The Debye Scherer equation was used to calculate size (*D*) as shown table1 , and the Bragg rule was used to determine the distance between atoms, as stated in the equations"[11]":

$$D = 0.9\,\lambda/\beta\cos\theta \quad (1)$$

$$n\lambda = 2d\sin\theta \quad (2)$$

Where λ: represents the wavelength of x-rays and is equal to (1.54 nm).
θ: diffraction angle, d: the distance between the atoms,
β: the width of the angled line at mid-high

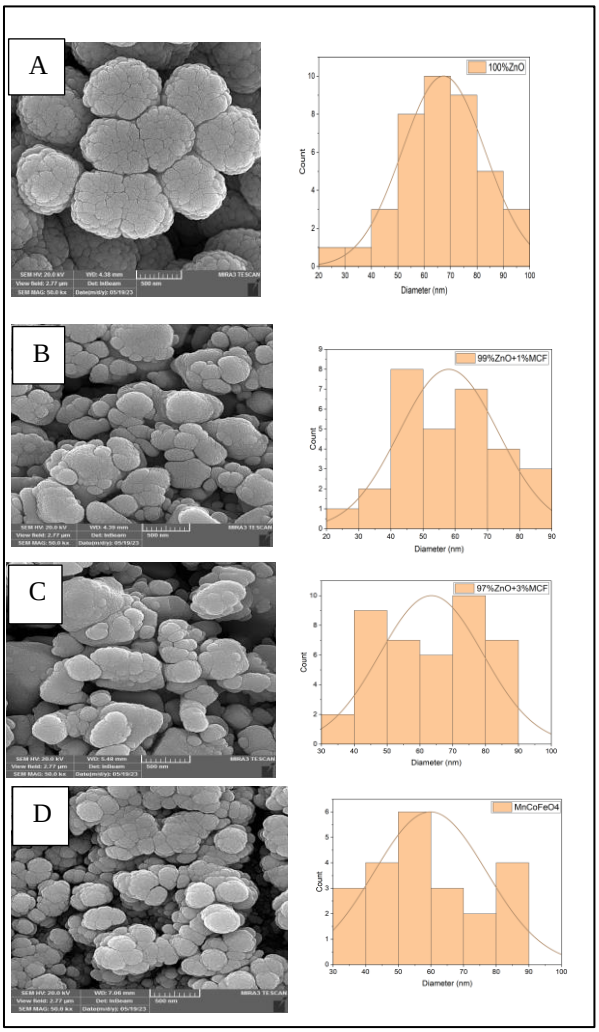

"Fig.2": A-SEM image of 500nm scale of Zno film
B-SEM image of 500nm scale of (99%ZnO+1%MnCoFeO4) film
C-SEM image at500nm scale of (97%ZnO+3%MnCoFeO4) film
D-SEM image of 500nm scale of MnCoFeO4 (left).
The corresponding particles size distribution (right)

*Table (*1) : the average particle sizes (D) and -spacing

sample	***D(nm)***	***d-speacing (A)***
100% ZnO	38.5	2.6
97%ZnO+3%MCF	24.7	2.5
$MnCoFeO_4$	8.7	2.04
Pt	9.1	1.8

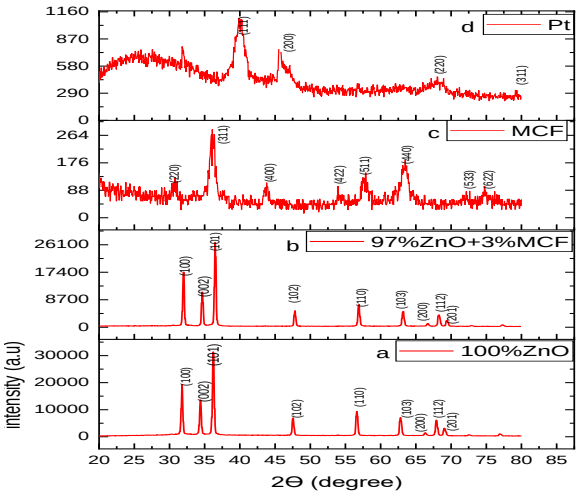

Fig. 3: XRD for thin films of (100% ZnO) , (97%ZnO+3%$MnCoFeO_4$), (Pt) and $MnCoFeO_4$

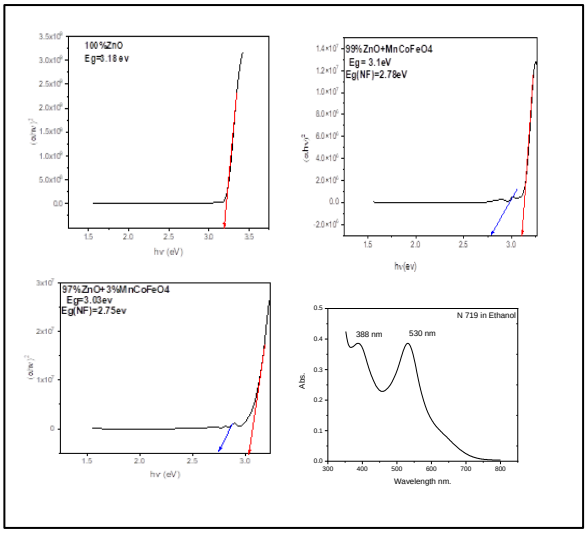

Fig. 4: UV -Vis of Pure and doped zinc oxide films and absorption peaks for the dyeN719

C. UV-Vis absorption spectra analysis

By using (*UV-Vis*) optical measurements, the energy gaps for samples of both pure and doped zinc oxide (*$MnCoFeO_4$*) with doping percentages (1% and 3%) were determined. “Fig (4)” displays the (3.22 eV) energy gap for pure (*ZnO*)[12],as well as the notable reduction in its values caused by doping, which was the primary factor contributing to the improvement in current, voltage, and efficiency of the cell It was found that the absorption of UV light is significant, in contrast to the absorption in the visible range, which is minimal, because there are more electrons being transported from the excited levels to the conduction band of the semiconductor[13],The energy gap was also calculated for (*$MnCoFeO_4$*) whose value was between (2.75-2.8 eV), As for the dye N719, two peaks appeared at (388-530) nm. It reason for the appearance of the absorption peak at (388 nm) is due to the electronic transition from the ground state (S_0) to the mono-excited state (S_2), while the appearance of the absorption peak at wavelength (530 nm) is due to the electronic transition from the ground state (S_0) to the Excited single state (S_1) and these transitions are of the allowed type and the optical energy gap has been calculated for it (Eg= 2.01eV) from the application of equation “(3)”:

$$Eg = 1240 / \lambda \text{ (nm)} \qquad (3)$$

D. Analysis of magnetization characteristics

The magnetic properties of the fabricated photoanode in powder form were characterized by the vibrated sample magnetometer (*VSM*) [*MDK Iran*] device with very careful and precise protocol of measurements. Remanence magnetization (*Mr*), coercivity forces (*Hc*), and saturation magnetizations (Ms) are three quantities that are used for describing magnetism in materials. Magnetic strength of the material in the absence of an external magnetic field is measured by the (*Mr*) value. The ability of a substance with magnetic properties to remain magnetized in an external field is determined by the coercivity force or the value (*Hc*). The maximum product of an induced magnetization value and the corresponding applied field is denoted by the symbol (*BH*) max. Although many magnetic materials retain either a high (*Mr*) value or a high (*Hc*) value but not both, a high (*Mr*) value or a high (*Hc*) value does not imply a high (BH) max value. The magnetic hysteresis loops of the samples show that zinc oxide is affected by the magnetic properties of the added impurities, and thus the values of saturation magnetization *(Ms*), remanence magnetization (*Mr*), and coercive field (*Hc*). The magnetic hysteresis curves in “Fig 5a” shows very slight magnetic behavior of pure (*ZnO*) of soft ferro-like remanence magnetization which might be due Zinc and/or oxygen vacancies or might be due defects. Numerous striking results about the intrinsic nanostructured ZnO's ferromagnetic nature have shown that point defects such Zn vacancies (V_{Zn}), Zn interstitials (Z_{ni}), and oxygen vacancies (V_O) have a significant impact on the magnetic characteristics[14].In 3.67, 4.52, and 6.30 nm undoped ZnO nanoparticles, X. Xu et al. revealed size dependence of defect generated room temperature ferromagnetism and demonstrated that smallest nanoparticles have the greatest magnetization. It is known that singly charged oxygen vacancies play a major role in

the magnetism of these materials[15][16].The hysteresis loop of (*95%ZnO+5%MnCoFeO₄*) is depicted in Figure 5b. The height and the broadening of the hysteresis loop in "Fig 5b" indicate an increase in the magnetic parameters, which is much larger than that of pure (*ZnO*). Sample (*95%ZnO+5%MnCoFeO₄*) behave like ferromagnet or precisely as a diluted magnetic semiconductor (*DMS*). The value of the Coercive field (*Hc*),(*Ms*) and (*Mr*) is depicted in table (2).

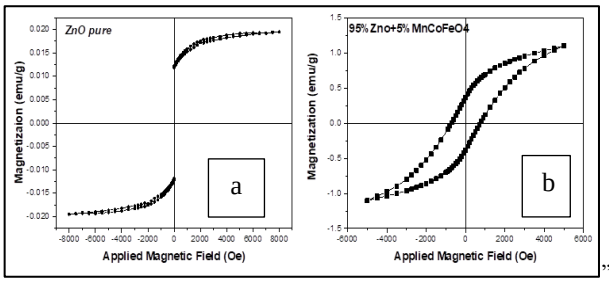

Fig.5: Hysteresis loops; magnetic field versus magnetization graph for a-(ZnO) and b-(ZnO+$MnCoFeO_4$)

" Table 2": Magneto metric parameters of the pure and doped ZnO nanoparticle

Samples	Saturation magnetization (emu/g)	Remanence Magnetization (emu/g)	Coercive Field (Oe)
100%ZnO	0.0194	0.0122	0
95%ZnO+5%MCF	1.103	0.414	746

E. Photovoltaic Measurements (I-V)

Measurements were made for a set of solar cells based on pure and doped zinc oxide with ratios (1,2,3,4,5) %from (*$MnCoFeO_4$*) which is shown in table (3). We observed that after doping, there are a gradual increase in efficiency, voltage, and current. We get the highest efficiency when doping with a ratio of (3%), but other than this percentage, that is, at (4,5) %. there is a decrease in cell efficiency, The reason for the increase is due to the Hall effect on the cell [17], that is, when the magnetic field is applied on the cell, an electromagnetic force is generated perpendicular to the current, which leads to an increase in the separation process of (electron-hole) pairs, that is, an increase in the transmission of free electrons at the photoanode electrode. The other reason for this increase is the presence of dye (N719), which contains within its composition the heavy element ruthenium, which contains the triple levels, as strong coupling occurs between (spin-orbit), which accelerates the process of crossing between systems[18] N719 dye converts incident solar light into a wavelength equivalent to its absorption spectrum, which causes an increase in cell efficiency[19]. As well as the grinding process that took place between zinc oxide and (*$MnCoFeO_4$*) provided a large area due to the small particle size to absorb the dye molecules more and thus increase the number of electrons transferred to the photoanode[20]. As for the reason for the decrease in efficiency when doping at (4,5)% is the increase in the content of the magnetic substance added to the zinc oxide, which led to a decrease in the electrical properties [21] result of the difference between the density of the zinc oxide particles and (*$MnCoFeO_4$*),The "fig (8)" shows curves (*I-V*) under a light of intensity of 100 "mw/cm^2",it is area 1cm^2, The current density, the open circuit voltage and the filling factor were measured. As for the efficiency, they were calculated by applying the following equations" [22]":

$$\eta = P_{out} / P_{in} = J_{sc} * V_{oc} * F.F / P_{in} \qquad (4)$$

J_{sc}: current density, V_{oc}: photovoltaic open circuit voltage, F.F: cell fill factor, P_{in}: The intensity of the incident light

$$IV.\ F.F = V_{MAX} * I_{MAX} / V_{OC} * I_{SC} \qquad (5)$$

$$P_{max} = V_{max} * I_{max} \qquad (6)$$

The Figure (6) shown the dependence the current density of DSSCs on the percentage of MCF, its clear there is increasing in the current with increasing of MCF where the 3% it's shows maximum current obtained after that there is drop in current density (for 4% and 5%), that can be attributed to increasing in charge carriers separation process and/or decreased recombination occur through the internal magnetic effect the electron-hole pairs of the organic dye [23] .

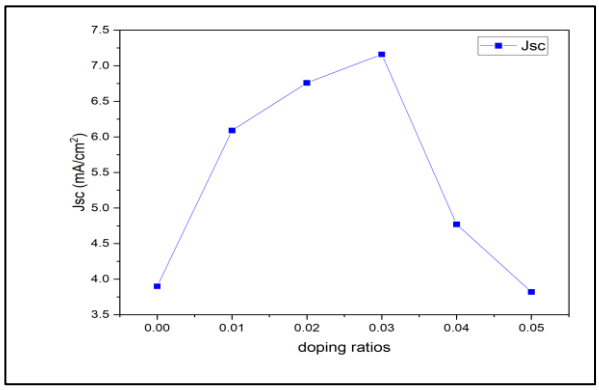

"Fig.6": The effect of doping ratios on current density

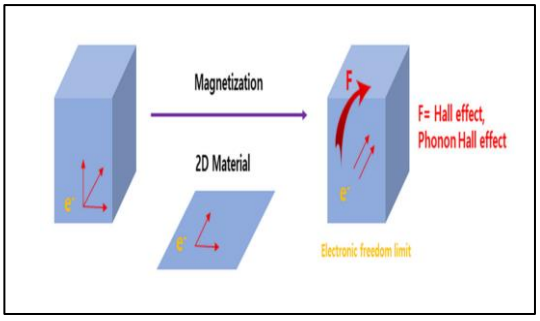

"Fig 7": the mechanism of the process for the charges after applied Magnetic Field

"Table. 3" : Results of solar cells with incorporation of magnetic nanoparticles

samples	J_{sc} (mA/cm^2)	V_{oc} (mV)	P_{max} (mw/cm^2)	F.F	η (%)
100%ZnO	3.9	530	1.39	0.67	1.38
99%ZnO+1%MCF	6.09	536.2	1.63	0.5	1.63
98%ZnO+2%MCF	6.76	553.1	1.57	0.42	1.57
97%ZnO+3%MCF	7.16	576.2	1.73	0.42	1.7
96%ZnO+4%MCF	4.77	552.6	1.57	0.59	1.55
95%ZnO+5%MCF	3.82	546.3	1.37	0.65	1.35

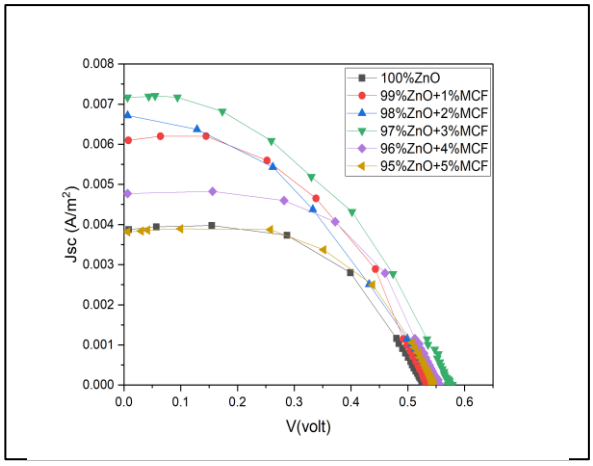

"Fig.8": DSSCs (I-V) characteristic Curves

V. Conclusions

In brief, this work focused solely on examining photocurrent generation processes in dye-sensitized solar cells. We selected the pure and doped ZnO photoanode with magnetic nanoparticles for comparison. The obtained results show considerable enhancement in photocurrent doped sample comparing with the cell of pure ZnO photoanode. This might be due to increased charge carriers' separation process and/or decreased recombination occurs through the internal magnetic effect the electron-hole pairs of the organic dye. This simple consideration indicates that it worth more investigations and factors that should be taken into account when developing new sensitizers.

Conflict of Interest

Authors declare that they have no conflict of interest.

References

[1] M. Grätzel, "Solar energy conversion by dye-sensitized photovoltaic cells," *Inorg. Chem.*, vol. 44, no. 20, pp. 6841–6851, 2005, doi: 10.1021/ic0508371.

[2] Y. K. Sanusi, A. A. Kazeem, and K. O. Suleman, "Photoanode Thickness and Sensitization Time Effects on Overall Performance of Nanocrystalline TiO2 Based Solar Cell Sensitized with Roselle Flower Extracts," *Int. J. Sci.*, vol. 7, no. 5, pp. 345–350, 2016.

[3] W. Shockley and H. J. Queisser, "Detailed balance limit of efficiency of p-n junction solar cells," *J. Appl. Phys.*, vol. 32, no. 3, pp. 510–519, 1961, doi: 10.1063/1.1736034.

[4] Rahmayeni, A. Devi, Y. Stiadi, N. Jamarun, Emriadi, and S. Arief, "Preparation, characterization of ZnO/CoFe2O4 magnetic nanocomposites and activity evaluation under solar light irradiation," *J. Chem. Pharm. Res.*, vol. 7, no. 9, pp. 139–146, 2015.

[5] H. Jabbar, B. A. Abdullah, and N. Ahmad, "Tuning TiO 2 Porosity of Multilayered Photoanode Towards Enhanced Performance of Dye Sensitized Solar Cell," *Al-Mustansiriyah J. Sci.*, vol. 33, no. 4, pp. 0–4, 2022.

[6] J. Barber and B. Andersson, "Revealing the blueprint of photosynthesis," *Nature*, vol. 370, no. 6484. pp. 31–34, 1994. doi: 10.1038/370031a0.

[7] N. Rajamanickam, S. S. Kanmani, K. Jayakumar, and K. Ramachandran, "On the possibility of ferromagnetism and improved dye-sensitized solar cells efficiency in TiO 2 /ZnO core/shell nanostructures," *J. Photochem. Photobiol. A Chem.*, vol. 378, no. March, pp. 192–200, 2019, doi: 10.1016/j.jphotochem.2019.04.042.

[8] Y. M. Xiao *et al.*, "Low temperature fabrication of high performance and transparent Pt counter electrodes for use in flexible dye-sensitized solar cells," *Chinese Sci. Bull.*, vol. 57, no. 18, pp. 2329–2334, 2012, doi: 10.1007/s11434-012-5110-6.

[9] R. Elshypany *et al.*, "Elaboration of Fe3O4/ZnO nanocomposite with highly performance photocatalytic activity for degradation methylene blue under visible light irradiation," *Environ. Technol. Innov.*, vol. 23, 2021, doi: 10.1016/j.eti.2021.101710.

[10] S. Agarwal, L. K. Jangir, K. S. Rathore, M. Kumar, and K. Awasthi, "Morphology-dependent structural and optical properties of ZnO nanostructures," *Appl. Phys. A Mater. Sci. Process.*, vol. 125, no. 8, 2019, doi: 10.1007/s00339-019-2852-x.

[11] K. C. B. Naidu and W. Madhuri, "Hydrothermal synthesis of NiFe2O4 nano-particles: Structural, morphological, optical, electrical and magnetic

properties," *Bull. Mater. Sci.*, vol. 40, no. 2, pp. 417–425, 2017, doi: 10.1007/s12034-017-1374-4.

[12] A. Baouid, S. Elhazazi, A. Hasnaoui, P. Compain, J. P. Lavergne, and F. Huet, "Highly peri-, regio- and diastereoselective 1,3-dipolar cycloaddition of mesitonitrile oxide to 1,7-dimethyl-2,3-dihydro-1H-1,4-diazepines: Unexpected one-step formation of a new triheterocyclic framework," *New J. Chem.*, vol. 25, no. 12, pp. 1479–1481, 2001, doi: 10.1002/chin.200229170.

[13] S. Munir *et al.*, "Nickel ferrite/zinc oxide nanocomposite: Investigating the photocatalytic and antibacterial properties," *J. Saudi Chem. Soc.*, vol. 25, no. 12, p. 101388, 2021, doi: 10.1016/j.jscs.2021.101388.

[14] X. Xu, C. Xu, Y. Lin, J. Li, and J. Hu, "Comparison on photoluminescence and magnetism between two kinds of undoped ZnO nanorods," *J. Phys. Chem. C*, vol. 117, no. 46, pp. 24549–24553, 2013, doi: 10.1021/jp405662y.

[15] U. Routray, R. Dash, J. R. Mohapatra, J. Das, V. V. Srinivasu, and D. K. Mishra, "Temperature-dependent ferromagnetic behavior in nanocrystalline ZnO synthesized by pyrophoric technique," *Mater. Lett.*, vol. 137, pp. 29–31, 2014, doi: 10.1016/j.matlet.2014.08.109.

[16] S. Pattanaik, B. Biswal, U. Routray, J. Mohapatra, V. V. Srinivasu, and D. K. Mishra, "Oxygen vacancy induced ferromagnetism in ball milled Zn0.97Ni0.03O: Confirmation through electron spin resonance," *Mater. Today Proc.*, vol. 35, no. xxxx, pp. 141–144, 2021, doi: 10.1016/j.matpr.2020.03.547.

[17] D. A. Shalybkov and V. A. Urpin, "The hall effect and oscillating decay of a magnetic field," *Tech. Phys.*, vol. 45, no. 2, pp. 147–152, 2000, doi: 10.1134/1.1259587.

[18] F. Cai, S. Zhang, and Z. Yuan, "Effect of magnetic gamma-iron oxide nanoparticles on the efficiency of dye-sensitized solar cells," *RSC Adv.*, vol. 5, no. 53, pp. 42869–42874, 2015, doi: 10.1039/c5ra05936d.

[19] B. Govindarajan, R. Palanimuthu, and K. M. Manikandan, "Influence of Mg doping in magnetic properties of NiO nanoparticles and its electrical applications," *J. Mater. Sci. Mater. Electron.*, vol. 30, no. 7, pp. 6519–6527, 2019, doi: 10.1007/s10854-019-00957-2.

[20] H. S. E. Kouhestanian, M. Ranjbar, S. A. Mozaffari, "Investigating the Effects of Thickness on the Performance of ZnO-Based DSSC," *Iran. Res. Organ. Sci. Technol.*, vol. 14, pp. 101–112, 2021.

[21] H. S. Kang, W. S. Kim, Y. K. Kshetri, H. S. Kim, and H. H. Kim, "Enhancement of Efficiency of a TiO2-BiFeO3 Dye-Synthesized Solar Cell through Magnetization," *Materials (Basel).*, vol. 15, no. 18, 2022, doi: 10.3390/ma15186367.

[22] Q. Zhang, C. S. Dandeneau, X. Zhou, and C. Cao, "ZnO nanostructures for dye-sensitized solar cells," *Adv. Mater.*, vol. 21, no. 41, pp. 4087–4108, 2009, doi: 10.1002/adma.200803827.

[23] E. Frankevich and A. Zakhidov, "Photoconductivity of poly „ 2 , 5-diheptyloxy- p -phenylene vinylene … in the air atmosphere : Magnetic-field effect and mechanism of generation and recombination of charge carriers," *Inst. Mol. Sci. Myodaiji, Okazaki, 444, Japan*, vol. 53, no. 8, pp. 4498–4508, 1996.